Transverse Compressive Properties of Carbon/Glass Hybrid Thermoplastic Composite Rods

Kimiyoshi Naito, Chiemi Nagai, and Yoshihisa Tanaka

Research Center for Structural Materials, Polymer Matrix Hybrid Composite Materials Group, National Institute for Materials Science (NIMS), Tsukuba, Ibaraki, 305-0047, Japan

Abstract: Novel carbon/glass hybrid thermoplastic composite rods having different carbon/glass ratios (24K1P, 24K2P, and 24K3P) are commercially fabricated. The transverse compressive properties of these three hybrid rods were investigated. The load-displacement curve showed large nonlinear behavior and a complicated shape. In the initial stage, the load gradually increased by increasing the deformation. In the second stage, the load-displacement relation was almost linearly proportional to the displacement (stable deformation region). Subsequently, the slope decreased slightly, before the load-displacement curve showed a clear slope increase as the deformation proceeded. The fracture behavior of the hybrid rods was examined using a digital microscope. The observed fracture paths formed almost straight lines running through the loading point, the center of the cross section of carbon fiber bundles/thermoplastic epoxy, as well as the interface between the glass fiber bundles/thermoplastic epoxy and the carbon fiber bundles/thermoplastic epoxy.

Key words: Carbon fiber, glass fiber, thermoplastic epoxy, hybrid, transverse compressive properties.

Nomenclature

24K1P:	hybrid rod having one carbon fiber bundle of 24,000 filaments
24K2P:	hybrid rod having two carbon fiber bundles of 48,000 filaments
24K3P:	hybrid rod having three carbon fiber bundles of 72,000 filaments
DIC:	digital image correlation

Greek letters

d:	diameter
θ:	braid angle
ρ_h:	density
V_{CF}:	volume fraction of carbon fiber
V_{GF}:	volume fraction of glass fiber
V_M:	volume fraction of matrix
V_V:	volume fraction of void E_L: tensile modulus
ν_{LT}:	Poisson's ratio
$\sigma_{L.ult}$:	tensile strength
$\varepsilon_{L.ult}$:	failure strain
m_L:	Weibull modulus
α:	intercept (power law model)
β:	slop (power law model)

Corresponding author: Kimiyoshi Naito, Ph.D., group leader, research fields: composites, mechanical engineering. E-mail: NAITO.Kimiyoshi@nims.go.jp.

L:	length of the hybrid rod
P:	transverse compression load
U^*:	deformation
C_s:	system compliance
U:	true deformation
F:	compressive load per unit length
E_L:	longitudinal modulus
E_T:	transverse modulus
R:	radius of the hybrid rod
b:	half-width of contact zone
dF/dU:	slope (F-U curve)
σ_{TC}:	transverse compressive stress
σ_{TCi}:	transverse compressive strength
ε_x:	normal strain
ε_{xy}:	shear strain

1. Introduction

Tendons are widely used as tension members for civil infrastructure, buildings, and offshore engineering structures [1-4]. Tendons and traditional reinforced concretes use high-tensile-strength steel wires, bars, and rebars. Corrosion and fatigue of steel cables and classical steel reinforcing bars are serious issues [5-7]. Therefore, the use of fiber-reinforced polymer matrix composites (fiber-reinforced plastics),

particularly carbon fiber-reinforced polymer matrix composites is proposed [8-10]. A novel carbon/glass hybrid thermoplastic composite rods called "CABKOMA" have been developed by Komatsu Seiren Co., Ltd. Three types of hybrid rods having differing carbon/glass ratios (24K1P, 24K2P, and 24K3P) were fabricated.

Recently, Naito et al. characterized the morphology and tensile properties of the hybrid rods (24K1P, 24K2P, and 24K3P) under static and fatigue loading [11, 12]. The braiding angles, volume fractions of elements (carbon fiber, glass fiber, matrix, and void), tensile properties of each hybrid rod under static and fatigue loading are found. The results are summarized in the **Supporting Information**.

Additionally, it is necessary to characterize compressive and flexural properties of these hybrid rods to understand their structural features and mechanical properties. The rods/ropes are usually stored/fastened to reels. Flexural and/or transverse compressive forces occur in individual rods. When handling/installing these rods/ropes, flexural and/or transverse compressive forces also occur in individual rods.

Cables in the above civil infrastructure, buildings, and offshore engineering structures are usually used for a rope configuration having an amount of twist [1-7]. Twist is inserted in rods to give them coherence. In a rope without twist, the individual rods would spread out and separate from one another. The rope, thus, would lack coherent unity [13]. Twist is even more important when frictional forces are solely due to transverse forces. Frictional forces alone hold individual rods in the rope, and transverse forces develop when a rod wrapped in a helical path around other rods in the rope is put under tension.

In this present study, the transverse compressive properties of the three types of hybrid rods having differing carbon/glass ratios (24K1P, 24K2P, and 24K3P) were evaluated. The transverse compressive tests for the hybrid rods were performed through in situ observation using a digital microscope. The deformation and strain localization of the hybrid rods were evaluated using a digital image correlation (DIC) method.

2. Experimental Procedure

2.1 Materials

The novel carbon/glass hybrid thermoplastic composite rods consisting of unidirectional polyacrylonitrile-based carbon fiber bundle (T700SC-24000-50C, Toray Industries, Inc.), braids of E-class glass fiber bundle (ECG751/01ZY-95T, Nippon Electric Glass Co., Ltd.), and thermoplastic epoxy matrix were developed by the Komatsu Seiren Co., Ltd. Three types of hybrid rods having different carbon/glass ratios were fabricated and described as 24K1P (one carbon fiber bundle of 24,000 filaments), 24K2P (two carbon fiber bundles of 48,000 filaments), and 24K3P (three carbon fiber bundles of 72,000 filaments). Detail information about the hybrid rods can be found in the literatures [11, 12] and are shown in the **Supporting Information**.

2.2 Transverse Compressive Test

The hybrid rods were first wrapped using sticky tape for the cutting process. The hybrid rods were cut into length of 6.0 mm using a rotary cutting machine at 2500 rpm. The abrasive cutting wheel for non-ferrous metal (GC150NB, Heiwa Technica Co., Ltd.) was used. A polishing surface of high precision is needed to investigate the deformation behavior and strain variations of micro-scale on the hybrid rods. Although the embedding molding method for polishing of the metal materials has been carried out using a resin as a typical polishing technique, because the hybrid rods are sensitively subjected to damages due to heat and solution conditions, the pre-existing polishing method is not able to be applied to the hybrid rods. A new polishing tool, which can be directly polished without the fabrication damages, was developed to observe the transverse compression

behaviors under the original conditions of the rod. The cross section of the hybrid rods was polished using a novel polishing tool [14] for the auto-rotary polishing machine. The tool can simultaneously polish a lot of rods with the well-right angle under constant load and same polishing conditions. Finally, the lengths of the hybrid rods were $L = 5.0$ mm.

The transverse compressive tests for the hybrid rod were performed through in situ observation using a digital microscope (VHX-5000 and VH-ZST, Keyence) with a compression module system (5 kN load cell, Kammrath & Weiss GmbH).

Specimens were placed on a block indenter. The displacement was applied quasi-statically at a crosshead speed of 1.0 μm/sec to obtain the transverse compressive properties of the hybrid rods. In addition, the displacement after a predetermined amount of load was halted to allow the in situ digital microscope observation of the deformation. All tests were conducted in the laboratory environment at room temperature (at 23 ± 3°C and relative humidity of 50 ± 5%). Ten specimens were tested (continuous load condition: five specimens, predetermined load condition: five specimens).

The transverse compression test yielded a load, P, as a function of the deformation curve, U^*, up to failure. The calibration was performed by applying a compressive load without a sample to estimate the system compliance, C_s. The true deformation, U, is given as follows:

$$U = U^* - C_s P \qquad (1)$$

Studies by Ward et al. derived the deformation, U, in a circular cross-section fiber as a function of the transverse compressive load, P, for an anisotropic body [15-18]. The equation is as follows:

$$U = \frac{4F}{\pi}\left(\frac{1}{E_T} - \frac{v_{LT}^2}{E_L}\right)\left(0.19 + \sinh^{-1}\frac{R}{b}\right) \quad (2)$$

where

F = compressive load per unit length ($= \dfrac{P}{L}$);

E_L = longitudinal modulus ($= E_{LC}$);

E_T = transverse modulus ($= E_{TC}$);

v_{LT} = Poisson's ratio;

R = radius of the hybrid rod ($= \dfrac{d}{2}$);

b = half-width of contact zone and is given as follows:

$$b = \sqrt{\frac{4FR}{\pi}\left(\frac{1}{E_T} - \frac{v_{LT}^2}{E_L}\right)} \qquad (3)$$

The transverse compressive modulus, E_{TC}, was calculated from Eq. (2) and the F-U curve obtained from the transverse compression test.

The diameter (d) of the hybrid rod was measured in previous studies using a micrometer [11, 12]. The average diameters of the hybrid rods are summarized in **Supporting Information** [11, 12]. The volume fraction of carbon fiber (V_{CF}), glass fiber (V_{GF}), matrix (V_M), void (V_V), and the tensile properties (tensile modulus (E_L), Poisson's Ratio (v_{LT}), tensile strength ($\sigma_{L.ult}$), failure strain ($\varepsilon_{L.ult}$), and Weibull modulus (m_L) in each type of hybrid rod are also shown in **Supporting Information** [11, 12].

3. Results and Discussion

3.1 Load-Displacement Curve

Fig. 1 shows the typical transverse compressive load per unit length-displacement (F-U) curves for
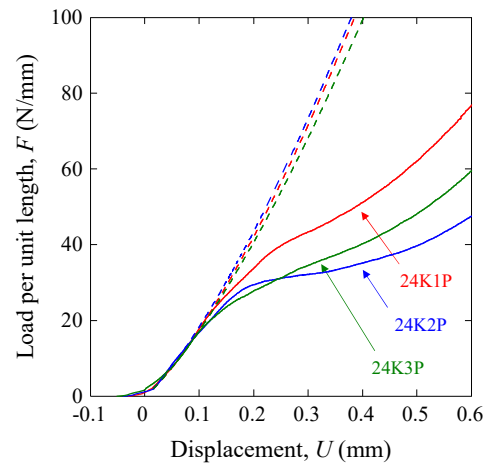

Fig. 1   Typical transverse compressive load per unit length-displacement curves for the hybrid rods.

the hybrid rods. The figures also depict the line obtained from Eq. (2) by curve fitting.

The F-U curves showed large nonlinear behavior and complicated shape. In the initial stage, the load gradually increased by increasing the deformation. This behavior was caused by the increase in the contact zone. In the second stage, the load-displacement relation was fitted by the analytical relation obtained from Eq. (2) (stable deformation region). Subsequently, the slope dF/dU decreased slightly. Finally, the load-displacement curve showed a clear increase in slope dF/dU as the deformation proceeded. The hybrid rods did not exhibit perfect circularity and displayed unevenness on the surface. This influence was attributed to the contact width, which was not measured in the study. The effect of the error of contact width on the transverse compressive properties was indicated by the experimental displacement at the low load level. However, in the intermediate load level (stable deformation region), the experimental load-displacement relations for the hybrid rods agreed well with the analytical line obtained from Eq. (2). The effect of the error of contact width was neglected. The experimental displacement was shifted such that the experimental result fit the analytical line (there was zero displacement at zero load) obtained from Eq. (2) in the intermediate load level (stable deformation region). Therefore, negative displacement occurred at a zero load.

3.2 Transverse Compressive Modulus

As shown in Fig. 1, the transverse compressive modulus, E_{TC}, was calculated from the F-U curve obtained from the transverse compressive test. The results are summarized in Table 1.

The E_{TC} of the hybrid rods were determined as 0.655 (24K1P), 0.644 (24K2P), and 0.639 GPa (24K3P), respectively. Fig. 2 shows the relationship between the transverse compressive modulus and the volume fraction of carbon fiber, V_{CF}, obtained from the previous investigation [11, 12], and were shown in **Supporting Information**.

3.3 Transverse Compressive Strength

The transverse compressive stress, σ_{TC}, is given as follows:

$$\sigma_{TC} = \frac{F}{d} = \frac{P}{L \cdot d} \qquad (6)$$

Fig. 3 shows typical transverse compressive stress-displacement (σ_{TC}-U) curves for the hybrid rods.

The transverse compressive stress at which these tangent lines intersect is defined as the transverse compressive strength, σ_{TCi}. The results are summarized in Table 1. The transverse compressive strengths, σ_{TCi}, of the hybrid rods were measured as 15.26 (24K1P), 8.79 (24K2P), and 8.05 MPa (24K3P), respectively. Fig. 4 shows the relationship between the transverse compressive strength and the volume fraction of carbon fiber, V_{CF}, obtained from the previous investigation [11, 12], and were shown in **Supporting Information**. The tensile strength increased by increasing V_{CF}, while the σ_{TCi} decreased.

3.4 Fracture Behavior

Digital micrographs of cross-sectional views of the transverse compressive fractured surface of the hybrid rods are shown in Fig. 5. The observed fracture paths formed almost straight lines running through the

Table 1   Transverse compressive properties of the carbon/glass hybrid thermoplastic composite rods.

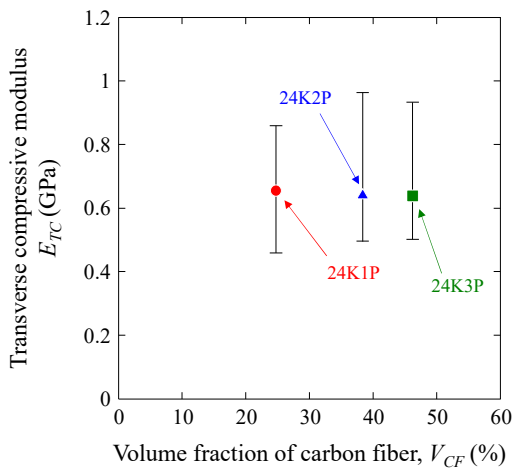|	24K1P	24K2P	24K3P
Transverse compressive modulus	0.655	0.644	0.639
E_{TC} (GPa)	(0.133)	(0.144)	(0.164)
Transverse compressive strength	15.26	8.79	8.05
σ_{TCi} (MPa)	(0.96)	(1.10)	(0.93)

( ) indicate standard deviations.

Fig. 2   Relationship between the transverse compressive modulus and the volume fraction of carbon fiber.
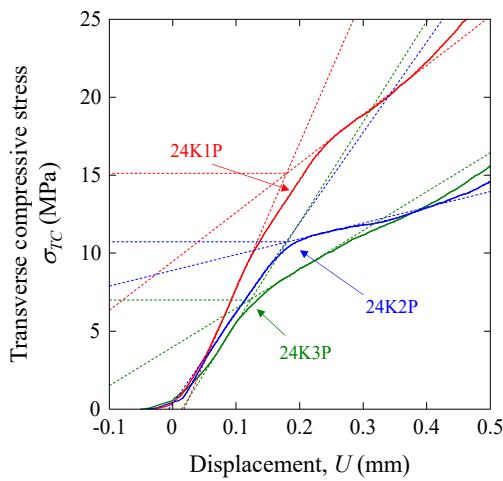

Fig. 3   Typical transverse compressive stress-displacement curves for the hybrid rods.
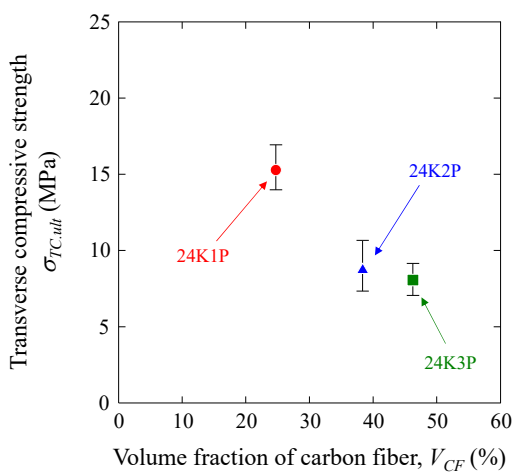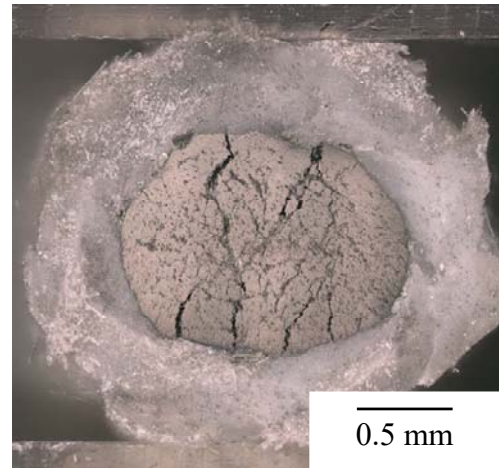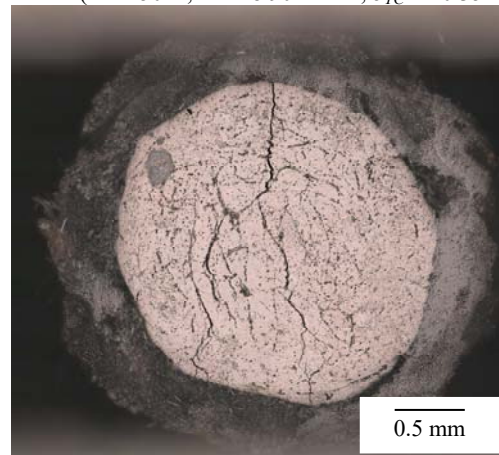

Fig. 4   Relationship between the transverse compressive strength and the volume fraction of carbon fiber.

(a) 24K1P (P = 200 N, F = 38.82 N/mm, σ_{TC} = 16.91 MPa)

(b) 24K2P (P = 150 N, F = 28.90 N/mm, σ_{TC} = 10.35 MPa)

(c) 24K3P (P = 150 N, F = 30.25 N/mm, σ_{TC} = 9.80 MPa)

Fig. 5   Digital microscope micrographs of cross-sectional views for the transverse compressive fractured surface of the hybrid rods.

loading point, the center of the cross section of the carbon fiber bundles/thermoplastic epoxy, as well as the interface between the glass fiber

bundles/thermoplastic epoxy and the carbon fiber bundles/thermoplastic epoxy.

3.4 Deformation and Strain Localization

The deformation and strain localization of the hybrid rods were measured using the morphology of the hybrid rods and evaluated using a DIC method. The two-dimensional DIC [19] obtained using the commercial software VIC-2D (Correlated Solutions, Inc.) [20] was used to analyze the localized displacement and strain distribution. Typical DIC conditions were set at subset size of 45 × 45 with seven pixel steps. A low-pass filter was used to minimize the influence of image noise. The thresholding levels were set at the maximum prediction margin of 0.02 pixels, with a 0.1 pixel maximum confidence interval using the covariance matrix of correlation equation.

Fig. 6 and Fig. 7 show the normal and shear strain contour maps, analyzed by the DIC method at magnifications of 500× for ε_x and ε_{xy}. The inhomogeneous deformation behavior appeared in the loading point, in addition to the center of the cross section of the carbon fiber bundles/thermoplastic epoxy as well as the interface between the glass fiber bundles/thermoplastic epoxy and the carbon fiber bundles/thermoplastic epoxy. The localized deformation was strongly dependent on the microstructures. The inhomogeneous deformations were local events such as matrix cracking, fiber/matrix interface debonding and sliding, and shear deformation. The averaged deformation almost linearly decreased with the distance from the loading point in the early deformation. By increasing applied displacement, inhomogeneous deformation appeared at the matrix between the fibers (carbon fiber
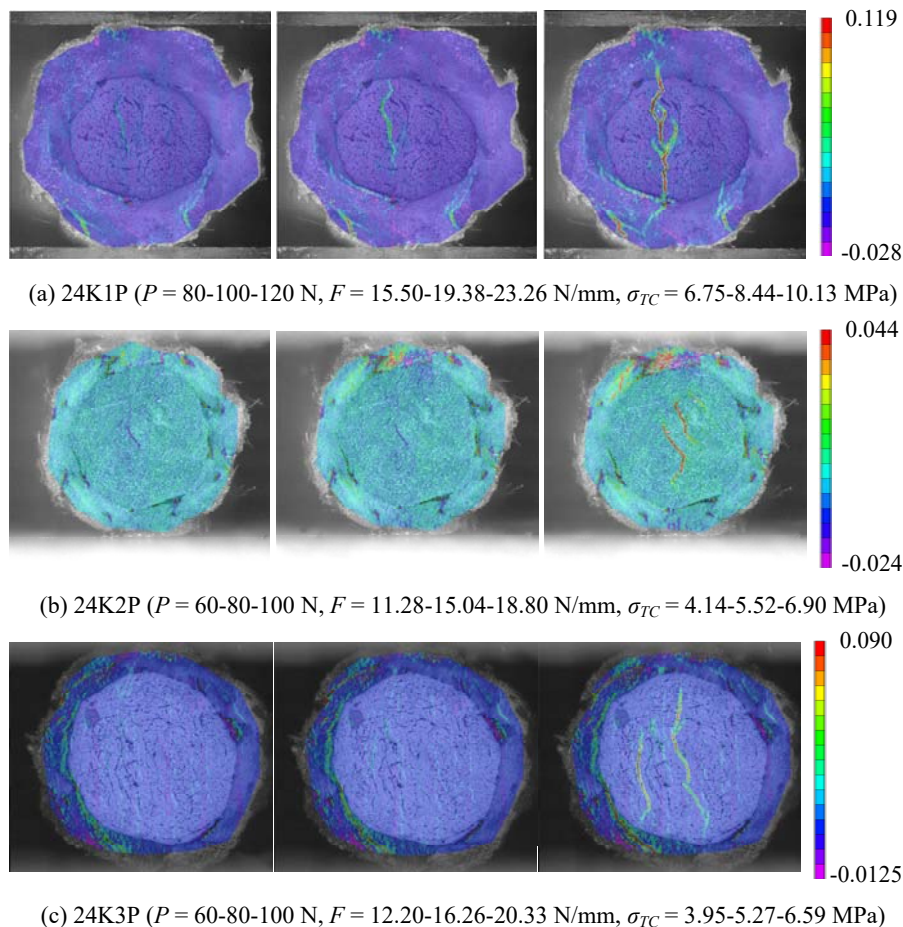

(a) 24K1P (P = 80-100-120 N, F = 15.50-19.38-23.26 N/mm, σ_{TC} = 6.75-8.44-10.13 MPa)

(b) 24K2P (P = 60-80-100 N, F = 11.28-15.04-18.80 N/mm, σ_{TC} = 4.14-5.52-6.90 MPa)

(c) 24K3P (P = 60-80-100 N, F = 12.20-16.26-20.33 N/mm, σ_{TC} = 3.95-5.27-6.59 MPa)

Fig. 6   Strain contour maps for ε_x.

(a) 24K1P (P = 80-100-120 N, F = 15.50-19.38-23.26 N/mm, σ_{TC} = 6.75-8.44-10.13 MPa)

(b) 24K2P (P = 60-80-100 N, F = 11.28-15.04-18.80 N/mm, σ_{TC} = 4.14-5.52-6.90 MPa)

(c) 24K3P (P = 60-80-100 N, F = 12.20-16.26-20.33 N/mm, σ_{TC} = 3.95-5.27-6.59 MPa)
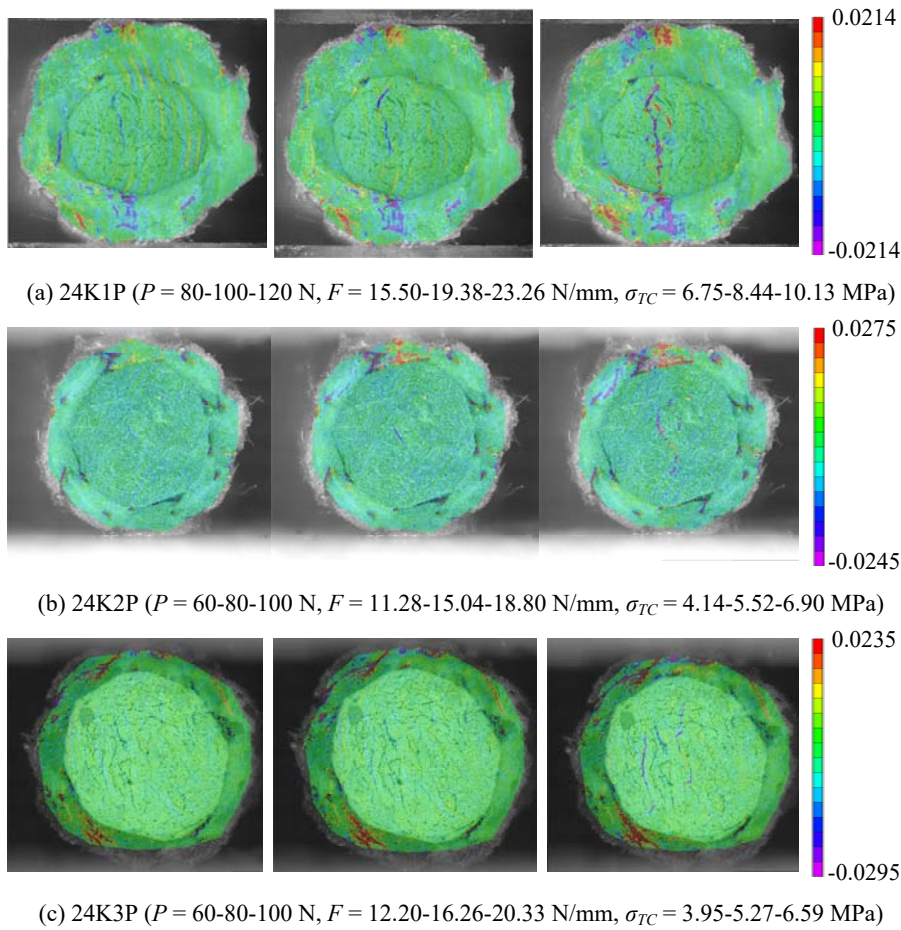
Fig. 7   Strain contour maps for ε_{xy}.

bundles/thermoplastic epoxy, glass fiber bundles/thermoplastic epoxy, as well as the interface between the glass fiber bundles/thermoplastic epoxy and the carbon fiber bundles/thermoplastic epoxy).

The localized tensile strain was present in the matrix between the fibers, despite the corresponding increase in the transverse compressive loading. The localized shear strain was also present in the matrix between the fibers. The results clearly demonstrate that the DIC method using the morphology pattern is important for measuring deformation and strain localization by identifying damage initiation and evolution.

4. Conclusions

The results of the transverse compressive tests of the hybrid rods are summarized as follows:

The load-displacement curve showed large nonlinear behavior and complicated shape. In the initial stage, the load gradually increased by increasing the deformation. In the second stage, the load-displacement relation was almost linearly proportional to the displacement (stable deformation region). Subsequently, the slope decreased slightly. Finally, the load-displacement curve showed a clear slope increase as the deformation proceeded.

The transverse compressive moduli of the hybrid rods were 0.655 (24K1P), 0.644 (24K2P), and 0.639 GPa (24K3P), respectively. Transverse compressive strengths of the hybrid rods were 15.26 (24K1P), 8.79 (24K2P), and 8.05 MPa (24K3P), respectively.

The observed fracture paths formed almost straight lines running through the loading point, the center of the cross section of the carbon fiber bundles/thermoplastic epoxy, as well as the interface between the glass fiber bundles/thermoplastic epoxy

and the carbon fiber bundles/thermoplastic epoxy.

The DIC method using the morphology pattern was important for measuring deformation and strain localization by identifying damage initiation and evolution.

Acknowledgments

References

[1]   Nawy, E. G. 2009. *Prestressed Concreate: A Fundamental Approach* (5th ed.). Prentice Hall, New York.

[2]   Soils & Structures. No. 220 Stay Cable. 2004. The Freyssinet group magazine.

[3]   Ocean structures: Ageing of offshore concrete structures. 2009. Petroleumstilsnet Petroleum safety authority Norway, OSL-804-R04-2.

[4]   Senjanovic, I., Tomic, M., and Rudan, S. 2013. "Investigation of Nonlinear Restoring Stiffness in Dynamic Analysis of Tension Leg Platforms." *Engineering Structures* 56 (11): 117-125.

[5]   Watson, S. C., and Stafford, D. 1988. "Cables in Trouble: Engineered Design and Construction." *Civil Engineering, ASCE* 58 (4): 38-41.

[6]   Périer, V., Dieng, L., Gaillet, L., Tessier, C., and Fouvry, S. 2009. "Fretting-fatigue Behaviour of Bridge Engineering Cables in a Solution of Sodium Chloride." *Wear* 267 (1-4): 308-314.

[7]   Hobbs, R. E., and Ghavani, K. 1982. "The Fatigue of Structural Wire Strands." *International Journal of Fatigue* 4 (2): 69-72.

[8]   Balaguru, P., Nanni, A., and Giancaspro, J. 2009. *FRP Composites for Reinforced and Prestressed Concrete Structures: A Guide to Fundamentals and Design for Repair and Retrofit*. Taylor, New York.

[9]   Meier, U. 2000. "Composite Materials in Bridge Repair." *Applied Composite Materials* 7 (2): 75-94.

[10] Maissen, A. 1997. "Concrete Beams Prestressed with CFRP Strands." *Structural Engineering International* 7 (4): 284-287.

[11] Naito, K., and Oguma, H. 2017. "Tensile Properties of Novel Carbon/Glass Hybrid Thermoplastic Composite Rods." *Composite Structures* 161 (2): 23-31.

[12] Naito, K., and Oguma, H. 2017. "Tensile Properties of Novel Carbon/Glass Hybrid Thermoplastic Composite Rods under Static and Fatigue Loading." *Revista Materia* 22 (2): e-11843.

[13] Hearle, J. W. S., Grosberg, P., and Backer, S. 1969. *Structual Mechanics of Fibers, Yarns, and Fabrics*. Wiley, New York.

[14] Choi, S. C., Tanaka, Y., Naito, K., and Kishimoto, S. 2014. Polishing method for polishing apparatus and polishing tool using holder for a rod shape specimen. Patent, No. 2014-259725 (Japanese).

[15] Hadley, D. W., Ward, I. M., and Wand, J. 1965. "The Transverse Compression of Anisotropic Fibre Monofilaments." In: *Proceedings of the Royal Society A: Mathematical, Physical & Engineering Sciences* 285 (1401): 275-286.

[16] Pinnock, P. R., Ward, I. M., and Wolfe, J. M. 1966. "Compression of Anisotropic Fibre Monofilaments. II." In: *Proceedings of the Royal Society A: Mathematical, Physical & Engineering Sciences* 291 (1425): 267-278.

[17] Jawad, S. A., and Ward, I. M. 1978. "The Transverse Compression of Oriented Nylon and Polyethylene Extrudates." *Journal of Materials Science* 13 (7): 1381-1387.

[18] Naito, K., Tanaka, Y., and Yang, J. M. 2017. "Transverse Compressive Properties of Polyacrylonitrile (PAN)-based and Pitch-Based Single Carbon Fibers." *Carbon* 118: 168-183.

[19] Pan, B., Qian, K., Xie, H., and Asundi, A. 2009. "Two-Dimensional Digital Image Correlation for In-Plane Displacement and Strain Measurement: A Review." *Measurement Science and Technology* 20 (6): 062001.

[20] Correlated Solutions Inc., VIC-2D, 952 Sunset Boulevard, West Columbia, SC 29252, USA. http://www.correlatedsolutions.com.

Table A Physical and tensile properties of the carbon/glass hybrid thermoplastic composite rods under static and fatigue loading.

	24K1P	24K2P	24K3P
Diameter d (mm)	2.30 (0.03)	2.73 (0.04)	3.09 (0.03)
Braid angle θ (°)	22.3 (1.6)	30.2 (1.5)	35.2 (1.8)
Density ρ_h (g/cm^3)	1.759 (0.007)	1.737 (0.008)	1.698 (0.009)
Volume fraction of carbon fiber V_{CF} (%)	24.58 (1.20)	38.34 (0.68)	46.18 (2.79)
Volume fraction of glass fiber V_{GF} (%)	39.75 (0.79)	29.63 (0.41)	23.15 (1.93)
Volume fraction of matrix V_M (%)	25.49 (0.37)	24.54 (0.32)	23.39 (0.67)
Volume fraction of void V_V (%)	10.18 (0.76)	7.49 (0.60)	7.28 (1.33)
Static test			
Tensile modulus E_L (GPa)	65 (3)	87 (7)	91 (7)
Poisson's ratio v_{LT}	0.39 (0.08)	0.41 (0.10)	0.45 (0.07)
Tensile strength $\sigma_{L.ult}$ (GPa)	1.42 (0.05)	1.80 (0.06)	1.84 (0.05)
Failure strain $\varepsilon_{L.ult}$ (%)	2.18 (0.07)	2.13 (0.15)	2.08 (0.14)
Weibull modulus m_L	23.77	27.29	32.50
Fatigue test $\sigma_{max} = \alpha \cdot \left(N_f\right)^{\beta}$			
Intercept (power law model) α	1.829	1.869	1.947
Slop (power law model) β	−0.1169	−0.0845	−0.0843

( ) indicate standard deviations.